

Cite this article as: Jiang Haiyang, Jiang Fuqing, Wang Bing, et al. Effects of Aging Treatment on Microstructure Evolution and Mechanical Properties of Ti-6Al-3Nb-2Zr-Mo Alloy[J]. Rare Metal Materials and Engineering, 2023, 52(06): 2002-2009.

ARTICLE

# Effects of Aging Treatment on Microstructure Evolution and Mechanical Properties of Ti-6Al-3Nb-2Zr-Mo Alloy

Jiang Haiyang<sup>1,2,3</sup>, Jiang Fuqing<sup>2,3</sup>, Wang Bing<sup>1,2,3</sup>, Xu Bin<sup>1,3</sup>, Sun Mingyue<sup>1,3</sup>

<sup>1</sup>Key Laboratory of Nuclear Materials and Safety Assessment, Institute of Metal Research, Chinese Academy of Sciences, Shenyang 110016, China; <sup>2</sup>School of Materials Science and Engineering, University of Science and Technology of China, Shenyang 110016, China; <sup>3</sup>Shenyang National Laboratory for Materials Science, Institute of Metal Research, Chinese Academy of Sciences, Shenyang 110016, China

**Abstract:** In order to understand the influence of the different aging parameters on the microstructure and mechanical properties of Ti-6Al-3Nb-2Zr-Mo (Ti6321) alloy, the microstructures and mechanical properties under different aging parameters (temperatures ranging from 500 °C to 650 °C, 3–24 h) were investigated by optical microscopy (OM), scanning electron microscopy (SEM), transmission electron microscopy (TEM), and mechanical properties tests. The results reveal that the secondary  $\alpha$  phase ( $\alpha_s$ ) is more sensitive to the aging parameters than the primary  $\alpha$  phase ( $\alpha_p$ ). Moreover, the thickness of  $\alpha_s$  phase is positively correlated with aging temperature or aging time. As the aging temperature and aging time increase, the segregation of Ti and Al elements in the  $\beta$  transformation phase ( $\beta$ ) becomes obvious, and the  $\alpha_s$  phase changes from fine needle-like to long rod-like. When the alloy is aged at 600 °C for 12 h, the alloy shows good comprehensive mechanical performance. The tensile strength, yield strength, and elongation are 907 MPa, 796 MPa, and 16%, respectively, and the impact energy is 55 J.

**Key words:** Ti-6Al-3Nb-2Zr-Mo titanium alloy; aging treatment; microstructure evolution; mechanical properties

Titanium alloys have a potential application in aerospace and marine engineering due to their high specific strength, excellent mechanical properties and corrosion resistance<sup>[1-3]</sup>. Ti-6Al-3Nb-2Zr-Mo (Ti6321) alloy is a near- $\alpha$  titanium alloy, which was developed by The Luoyang Ship Material Research Institute. It has unique properties and is specially designed for marine engineering applications<sup>[4-7]</sup>. However, the properties of titanium alloys depend on many factors such as composition, processing method, microstructure (such as crystal structure, grain size), and strengthening mechanism<sup>[8]</sup>. In general, the excellent mechanical properties of titanium alloys can be obtained through a series of thermomechanical processing (TMP) and heat treatment processes<sup>[9-11]</sup>. Moreover, heat treatment changes the properties of metal by changing its microstructure and subsequent mechanical properties<sup>[12]</sup>.

However, titanium alloy has very complex microstructure evolution characteristics during heat treatment. Among them,

the evolution of  $\alpha_p$  phase,  $\alpha_s$  phase,  $\beta$  phase and precipitates of titanium alloys have different effects on the strength, hardness, plasticity and toughness<sup>[13-14]</sup>. Therefore, it is very important to clarify the relationship between heat treatment, microstructure and mechanical properties<sup>[15]</sup>. In recent years, researchers have carried out a series of studies on the relationship between the heat treatment process and mechanical properties of titanium alloys. However, most studies are concerned on the effects of heat treatment process on microstructure and mechanical properties of  $\alpha+\beta$  titanium alloy and  $\beta$  titanium alloy. For example, Xavier et al<sup>[16]</sup> studied the effect of low temperature holding on the microhardness and microstructure of the dual phase titanium alloy Ti-15Zr-xMo. The results show that with the increase in the holding time, the content of  $\alpha'$  phase increases, which decreases the microhardness of the alloy. Wu et al<sup>[17]</sup> carried out heat treatment on Ti-6Al-4V in the temperature range from 300 °C

Received date: December 04, 2022

Foundation item: National Key Research and Development Program (2018YFA0702900); National Natural Science Foundation of China (52173305, 52101061, 52233017, 52203384); Strategic Priority Research Program of the Chinese Academy of Sciences (XDC04000000); China Postdoctoral Science Foundation (2020M681004, 2021M703276); IMR Innovation Foundation (2022-PY12); LingChuang Research Project of China National Nuclear Corporation; Youth Innovation Promotion Association, CAS

Corresponding author: Xu Bin, Ph. D., Professor, Key Laboratory of Nuclear Materials and Safety Assessment, Institute of Metal Research, Chinese Academy of Sciences, Shenyang 110016, P. R. China, Tel: 0086-24-83978839, E-mail: bxu@imr.ac.cn

Copyright © 2023, Northwest Institute for Nonferrous Metal Research. Published by Science Press. All rights reserved.

to 1020 °C and then the alloy was water quenched. It is found that there is a strong correlation between microstructure and hardness. The full  $\beta$  structure is obtained when the temperature rises over 900 °C, which shows the highest microhardness. Zhu et al<sup>[18]</sup> investigated the influence of heat treatment on microstructure and mechanical properties of TC17 titanium alloy. The results indicate that the grain boundary  $\alpha$  becomes thick after two-phase region solution and aging treatment. Zhou et al<sup>[19]</sup> found that the annealing temperature mainly affects the shape and volume fraction of the  $\alpha_p$  phase, and the alloy shows good comprehensive tensile properties when annealed at 930 °C for 1 h and aged at 600 °C for 4 h. Moreover, the research on the heat treatment of  $\beta$  titanium alloy mainly focuses on the relationship between the width of  $\alpha_s$  phase and temperature, especially the relationship between the microstructure and mechanical properties of the alloy after solution and aging treatment. Shekhar et al<sup>[20]</sup> studied the near- $\beta$  titanium alloy under  $\beta$  solution treatment and aging treatment, which can only obtain high strength. However, after  $\alpha+\beta$  solution treatment and aging treatment, the alloy shows the best combination of strength and plasticity. Du et al<sup>[13]</sup> found the relationship between the evolution of the  $\alpha_s$  phase in a new  $\beta$  titanium alloy after solution and aging treatment and mechanical properties. In addition, the research on heat treatment of  $\alpha$  titanium alloy mainly focuses on the cooling process, because  $\alpha$  titanium alloy is sensitive to cooling rate. For instance, it has been reported that cooling rate has a significant influence on the size of  $\alpha_s$  phase<sup>[21]</sup>, which leads to the change of the strength of titanium alloys<sup>[22]</sup>. Moreover, the change of the volume fraction of  $\alpha_p$  phase, size and morphology of  $\alpha_p$  phase during cooling process has also been reported. For example, Shi et al<sup>[23]</sup> found that with the decrease in the cooling rate, the volume fraction and diameter of the equiaxed  $\alpha$  and thicknesses of the lamellar  $\alpha$  will increase. In summary, some scholars have carried out numbers of researches on the heat treatment of titanium alloy. However, the study on heat treatment, microstructure evolution and mechanical properties of Ti6321 alloy is relatively scarce. So far, the effect of aging parameters on microstructure evolution and mechanical properties of Ti6321 alloy after solution treatment still remain unclear.

Therefore, in this work, the influence of aging process parameters on the microstructure evolution and mechanical properties of the Ti6321 alloy was investigated. Furthermore, the tensile and impact fracture mechanisms of the alloy after different aging treatments were analyzed. These findings may have theoretical guiding significance for industrial production.

## 1 Experiment

### 1.1 Materials and heat treatment process

The materials used in this study consisted of a  $\Phi 39$  mm $\times$ 80 mm Ti6321 forged bar, where the chemical composition (wt%) of Ti6321 was 3.01 Nb, 1.00 Mo, 1.95 Zr, 6.02 Al, 0.020 Si, 0.024 Fe, and balanced Ti. The  $\beta$  transus temperature was 990 °C. The solution treatment was carried out at 840 °C

for 1.5 h in an electricity-resistant furnace. The microstructure after solution treatment was composed of equiaxed and elongated  $\alpha_p$  phase and  $\beta_t$  phase, which was a typical bimodal structure (as seen in Fig. 1a). The  $\alpha_s$  phase can be clearly seen by the SEM observation, as shown in Fig. 1b. The mechanical properties of Ti6321 alloy after solution treatment are shown in Table 1.

After solution treatment, the cylindrical samples with  $\Phi 39$  mm $\times$ 80 mm were aged for 3, 6, 12 and 24 h in an electricity-resistant furnace at 500, 550, 600 and 650 °C. The heat treatment process is shown in Fig. 2.

### 1.2 Mechanical testing and characterization methods

The heat-treated cylindrical samples were processed for tensile and impact tests according to the sampling diagram shown in Fig. 3a, and the number of parallel samples was 3. The tested sample size is displayed in Fig. 3b–3c. All the tests were performed strictly according to the national standards, GB/T 228.1-2010 and GB/T 229-2007.

The microstructure of Ti6321 alloy, aged under different parameters followed by grinding, polishing, and etching (47 mL H<sub>2</sub>O+2 mL HNO<sub>3</sub>+1 mL HF) treatment, was observed through OM and a field-emission SEM. Moreover, the detailed microstructure information was obtained using a FESEM equipped with an energy dispersive spectroscopy

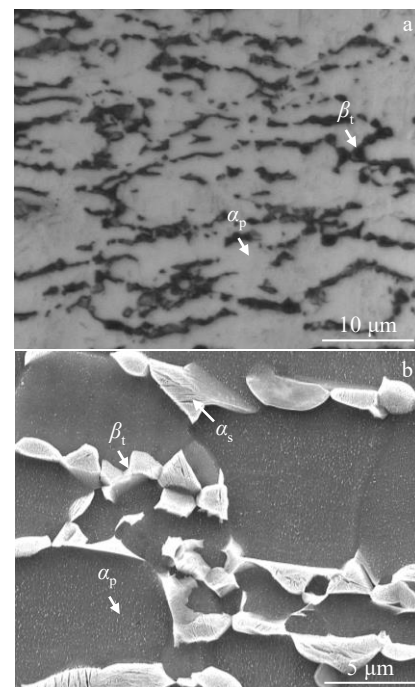


Fig.1 OM (a) and SEM (b) microstructures of Ti6321 alloy after solution treatment

Table 1 Mechanical properties of Ti6321 alloy after solution treatment

Ultimate strength/MPa	Yield strength/MPa	Elongation/%	Impact energy/J
887±14	763±15	15±0.9	51±1.5

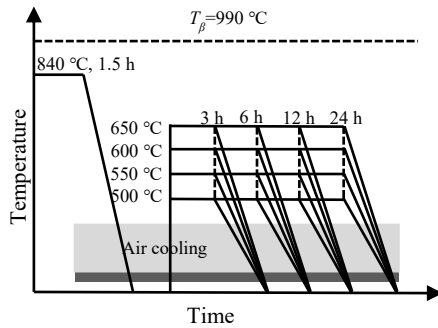


Fig.2 Heat treatment process of Ti6321 alloy

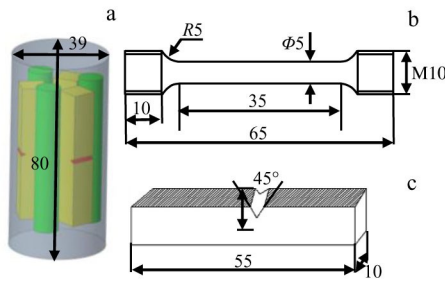


Fig.3 Schematics of the sampling for mechanical property test (a): (b) tensile test sample and (c) impact property test sample

(EDS). Furthermore, the fracture surface morphologies of the mechanically tested samples were investigated by SEM.

## 2 Results and Discussion

### 2.1 Effect of the aging parameters on microstructure of Ti6321 alloy

Fig.4 shows the microstructures of Ti6321 alloy after aging at 500–650 °C for 6 h. The microstructure of Ti6321 alloy still presents the typical bimodal microstructure after aging at different temperatures for 6 h. As the aging temperature increases, the content of  $\alpha_p$  phase does not change

significantly. However,  $\alpha_s$  is more sensitive to the aging temperature than  $\alpha_p$  phase. During the aging process, the  $\alpha_s$  phase is precipitated from the  $\beta_t$  phase. When aged at 500 °C for 6 h, the morphology of  $\alpha_s$  phases is fine needle-like, as shown in Fig. 4a<sub>1</sub>. As the aging temperature increases to 600 °C, the boundary of  $\alpha_s$  phase becomes clear and thick, and the morphology of  $\alpha_s$  phases changes into short rod-like, as shown in Fig. 4b<sub>1</sub> and Fig. 4c<sub>1</sub>. When the aging temperature reaches to 650 °C, the coarsening degree of  $\alpha_s$  phase reaches the maximum, and its morphology is long rod-like, as shown in Fig. 4d<sub>1</sub>.

Fig. 5 shows the high-angle annular dark-field scanning transmission electron microscope (HAADF – STEM) images and corresponding EDS mappings of the Ti6321 alloy aged at different temperatures for 6 h. Al is an element stabilizing the  $\alpha$  phase, which is enriched in the  $\alpha$  phase. In addition, Nb and Mo are elements that stabilize the  $\beta$  phase, so Nb and Mo are enriched in the  $\beta_t$  phase. Zr is a neutral element. HAADF-STEM results show that Ti and Al are mainly distributed in the  $\alpha_p$  phase. As the aging temperature increases, the element distribution in  $\beta_t$  phase changes obviously compared to  $\alpha_p$  phase. Under the condition of aging at 500 °C for 6 h, Nb and Mo elements are mainly enriched in  $\beta_t$  phase, as shown in Fig. 5a. However, as the aging temperature increases, the  $\alpha_s$  phase begins to precipitate from the  $\beta_t$  phase. Therefore, the segregation of Ti and Al elements appears in the  $\beta_t$  phase. Since the  $\alpha_s$  is a fine needle-shape, the segregation of elements is not obvious, as shown in Fig. 5b. Furthermore, as the aging temperature increases to 600 °C, the segregation of Ti and Al elements in  $\beta_t$  phase becomes obvious, as shown in Fig. 5c. When the aging temperature reaches to 650 °C, the segregation of Ti and Al elements appears obviously in  $\beta_t$  phase. At this time, the  $\alpha_s$  phase appears as long rod-like, as shown in Fig. 5d.

Fig. 6 show the microstructures of Ti6321 alloy after aging at 600 °C for 3, 12, and 24 h. As the aging time increases, the content of  $\alpha_p$  phase presents little change. After aging for 3 h, the  $\alpha_s$  phase is randomly distributed in  $\beta_t$ , and its morphology

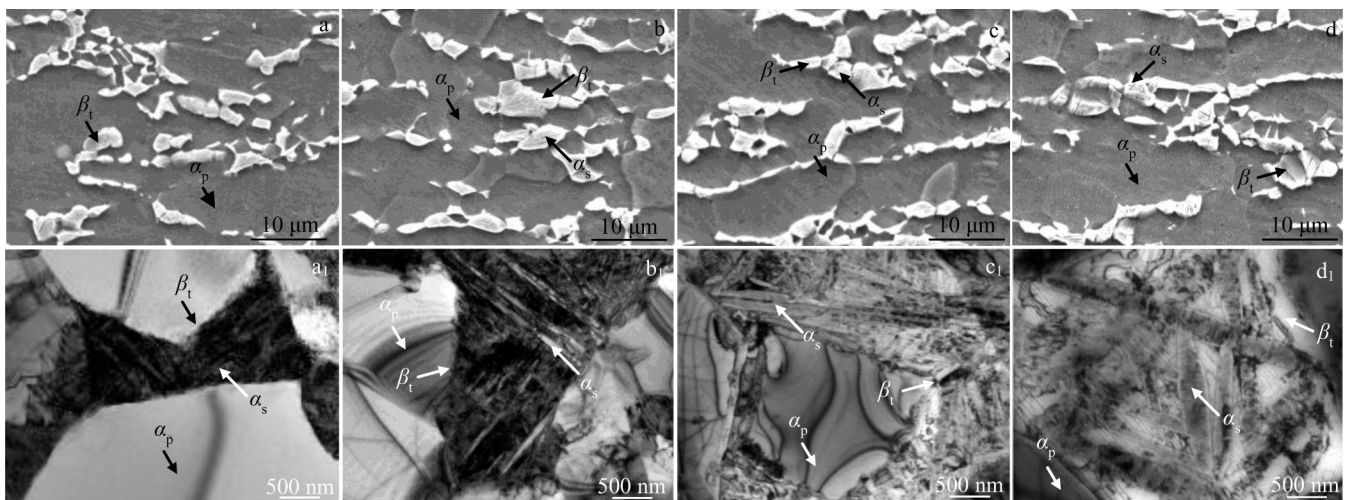


Fig.4 Microstructures of Ti6321 alloy aged at different temperatures for 6 h: (a, a<sub>1</sub>) 500 °C, (b, b<sub>1</sub>) 550 °C, (c, c<sub>1</sub>) 600 °C, and (d, d<sub>1</sub>) 650 °C

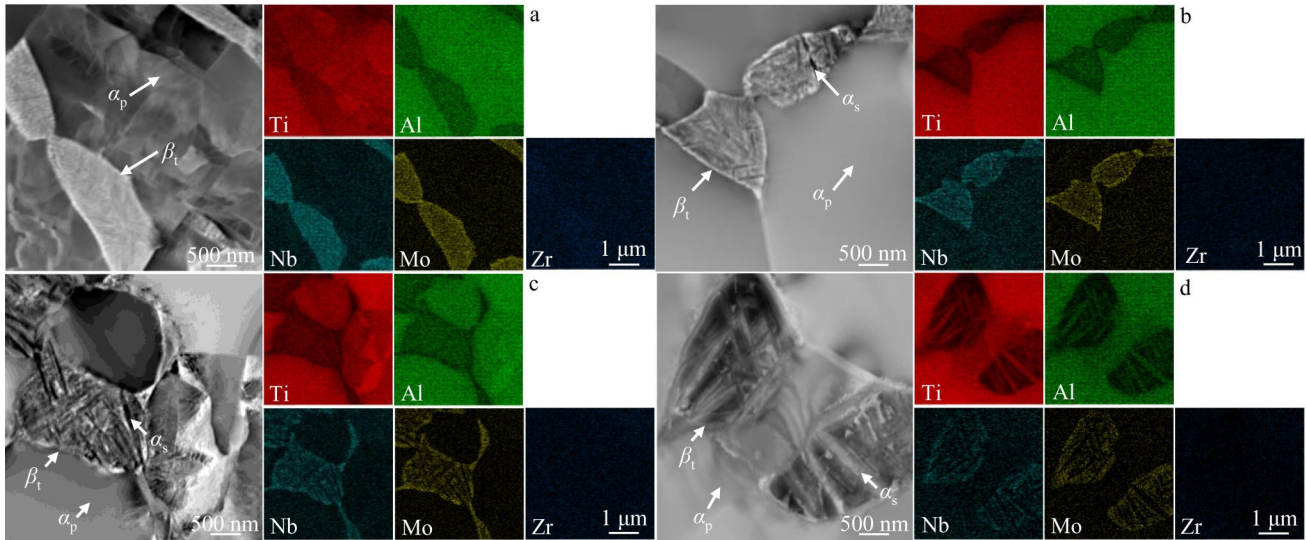


Fig.5 HAADF-STEM images and corresponding EDS mappings of Ti6321 alloy aged at different temperatures for 6 h: (a) 500 °C, (b) 550 °C, (c) 600 °C, and (d) 650 °C

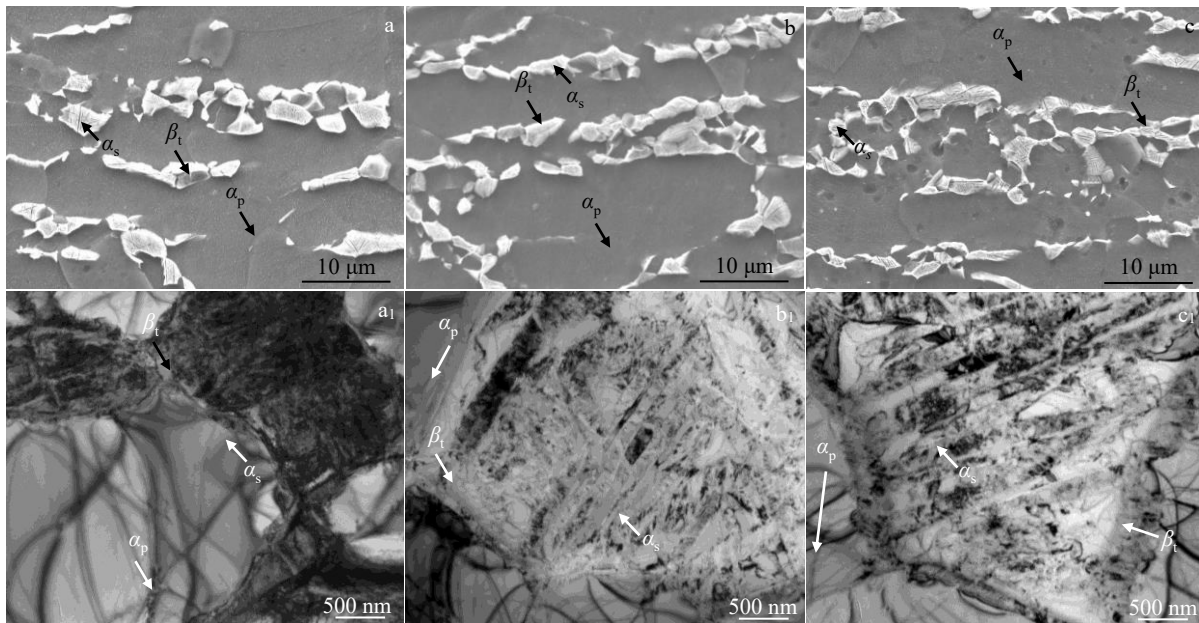


Fig.6 Microstructures of Ti6321 alloy aged at 600 °C for different time: (a, a<sub>1</sub>) 3 h, (b, b<sub>1</sub>) 12 h, and (c, c<sub>1</sub>) 24 h

is fine needle-like. Moreover, the  $\alpha_s$  phase boundary cannot be clearly identified, as shown in Fig.6a<sub>1</sub>. When the aging time increases to 6 h, the  $\alpha_s$  phase begins to grow, and its shape changes from fine needle-like to short rod-like. In addition, the  $\alpha_s$  phase boundary becomes distinct, as shown in Fig.4b<sub>1</sub>. When the aging time reaches to 12 h, the  $\alpha_s$  phase coarsens obviously. The shape of the  $\alpha_s$  phase changes into long rod-like, as shown in Fig.6b<sub>1</sub>. When the aging time is 24 h, the coarsening degree of  $\alpha_s$  phase reaches to the maximum. Meanwhile, the width of the  $\alpha_s$  phase becomes wider, and the boundary of  $\beta_t$  phase becomes fuzzy, as shown in Fig.6c<sub>1</sub>.

Fig.7 shows the HAADF-STEM images and corresponding EDS mappings of the Ti6321 alloy aged at 600 °C for

different time. HAADF-STEM results show that as the aging time increases, the element distribution in  $\beta_t$  phase changes obviously, and the distribution of elements in  $\alpha_p$  phase does not change significantly. After aging for 3 h, the segregation of Ti and Al elements appears in  $\beta_t$  phase, as shown in Fig.7a. However, when the aging time increases to 6 h, the segregation of Ti and Al elements in  $\beta_t$  phase becomes obvious, as shown in Fig.7b. When the aging time increases to 24 h, the segregation of Ti and Al elements appears in the  $\beta_t$  phase. Moreover, the  $\alpha_s$  phase grows and penetrates the  $\beta_t$  phase, and the morphology of  $\alpha_s$  shows a long rod-like, as shown in Fig.5d.

In conclusion, the coarsening of  $\alpha_s$  phase occurs with the

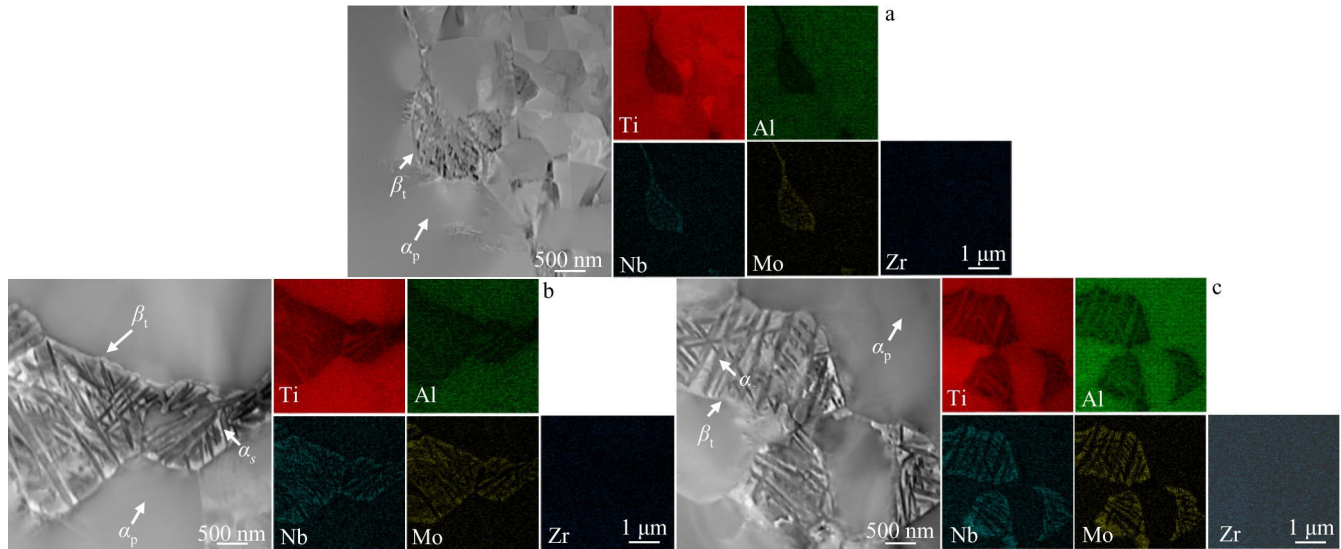


Fig.7 HAADF-STEM images and corresponding EDS mappings of Ti6321 alloy aged at 600 °C for different time: (a) 3 h, (b) 12 h, and (c) 24 h

increase in aging temperature and aging time. From the perspective of thermodynamics, the coarsening behavior of  $\alpha_s$  phase is a thermal activation process. Since the  $\beta_t$  phase is a metastable phase, the growth driving force of  $\alpha_s$  phase is provided with the increase in aging temperature, which promotes the coarsening of  $\alpha_s$  phase<sup>[24]</sup>. In addition, the coarsening rate of  $\alpha_s$  phase is controlled by the diffusion rate of solute atoms. The diffusion degree of solute atom is related to time. The longer the aging time, the more sufficient the diffusion of solute atoms, which will also promote the coarsening of the  $\alpha_s$  phase<sup>[25]</sup>. The schematic of the microstructure transformation is presented in Fig. 8. The yellow areas represent the  $\alpha_p$  phase, and the blue blocky regions represent the  $\beta_t$  phase, where the  $\beta_t$  phase consists of the  $\alpha_s$  phase. It can be clearly seen that with the increase in the aging temperature and aging time, the  $\alpha_s$  phase gradually grow and the width of the  $\alpha_s$  phases also increases, because  $\beta$  phase is transformed to the  $\alpha$  phase in aging process. In addition, after high temperature aging and longtime aging, the  $\alpha_s$  phase presents a complex change from fine needle-like to long rod-like.

## 2.2 Effect of aging parameters on mechanical properties of Ti6321 alloy

Fig. 9 shows the mechanical properties of Ti6321 alloy under different aging parameters. The red dotted line in Fig. 9 shows the mechanical properties of Ti6321 alloy after solution treatment. It can be seen that the ultimate tensile strength and yield strength after aging are significantly improved when the aging temperature is in the range of 500–600 °C. Once the aging temperature is increased to 650 °C, the strength decreases. In addition, when aging temperature increases up to 550 °C, the impact energy is higher than that of solution treated samples. Therefore, it is particularly important to find the suitable aging parameters to achieve the best combination between strength and toughness.

There are two factors that affect the tensile strength. On the

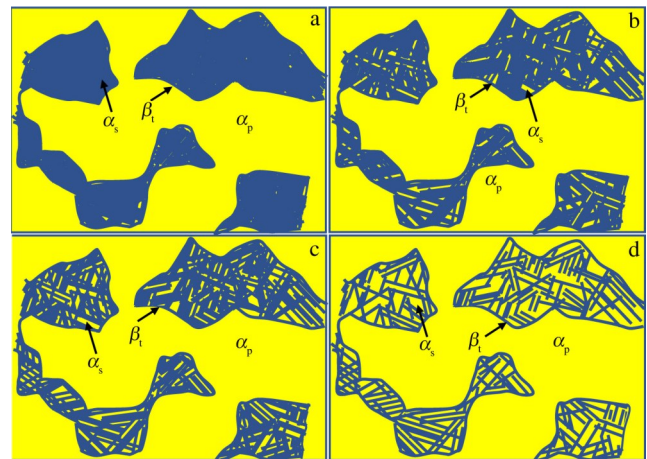


Fig.8 Schematic diagrams of microstructure transformation under different aging parameters

one hand, with the increase in aging temperature, the morphology of  $\alpha_s$  phase changes from fine needle-like to long rod-like, resulting in the decrease in interface area of  $\alpha_s$  phase boundary<sup>[26]</sup>, and finally decreasing the strength of the alloy, as shown in Fig. 9a and 9b. On the other hand, the spacing of the  $\alpha_s$  phase has an important influence on the strength of titanium alloy<sup>[24]</sup>. With the increase in aging temperature, the spacing of  $\alpha_s$  phase increases, resulting in decrease in the strength of alloy. As shown in Fig. 9a and 9b, with the increase in aging time, the strength basically shows a small trend. It indicates that the mechanical properties of the alloy are more sensitive to the aging temperature than that to aging time.

The impact toughness of titanium alloys has a significant influence on the distribution of  $\alpha_p$  phase, and size or morphology of  $\alpha_p$  phase. Generally speaking,  $\alpha_p$  phase is the channel of crack initiation and propagation<sup>[27]</sup>. Moreover, the thickness of  $\alpha_s$  phase has a great influence on the impact toughness of titanium alloys<sup>[24]</sup>. Appropriate thickness of  $\alpha_s$

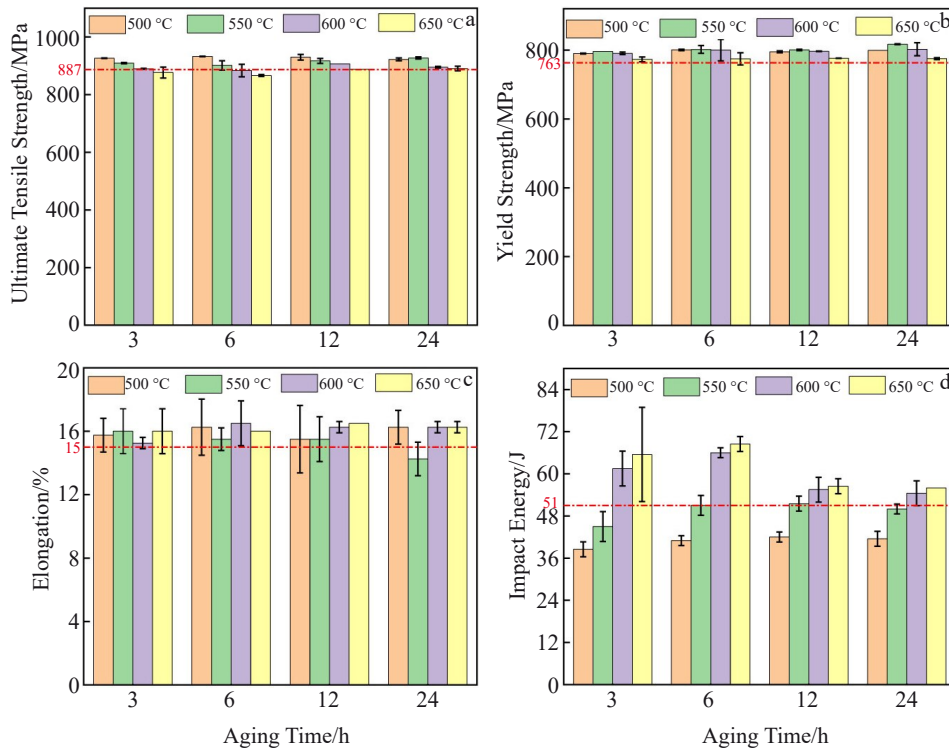


Fig.9 Mechanical properties of Ti6321 alloy after aging treatment: (a) ultimate tensile strength, (b) yield strength, (c) elongation, and (d) impact energy

phase can provide the best crack propagation resistance and high impact toughness. With the increase in aging temperature, the thickness of  $\alpha_s$  phase increases gradually, resulting in the increase in impact toughness. When the aging time is 6 h, the impact toughness reaches to the maximum value. The impact toughness begins to decrease after aging over 6 h, as shown in Fig.9d. It indicates that the thickness of  $\alpha_s$  phase at 6 h is the most conducive to hinder crack propagation, thereby improving the impact toughness of the material.

In summary, the alloy has the best comprehensive mechanical properties when aged at 600 °C for 12 h. The tensile strength, yield strength, and elongation are 907 MPa, 796 MPa, and 16%, respectively. Meanwhile, the impact energy is 55 J.

### 2.3 Impact and tensile fracture morphology analysis and fracture mechanism

Fig.10 shows the impact and tensile fracture morphologies of Ti6321 alloy after aging at different temperatures for 6 h. According to Fig.10a and Fig.10d, it can be seen from the macro fracture of the impact sample that the material shows ductile fracture. As can be seen from Fig.10a, the macro fracture gradually becomes uneven with the increase in aging temperature. Fig.10a<sub>1</sub> and Fig.10d<sub>1</sub> show the enlarged views of the position of the white dotted line frame. When the aging temperature is 500 °C, there are a large number of microvoids in the microscopic fracture. With the increase in aging temperature, the microvoids in the fracture are gradually reduced, and the dimple size is also reduced. Moreover, the

crack growth is affected by the lamellar structure. Meanwhile, the  $\alpha_s$  phase coarsens as the aging temperature increases. Therefore, the path of crack growth becomes tortuous and the resistance of crack growth increases, and finally the toughness of the material increases [28].

Fig.10e and Fig.10h show the macroscopic fractures of the tensile sample, and the material shows ductile fracture. Fig.10e<sub>1</sub> and Fig.10h<sub>1</sub> show the enlarged view of the position of the white dotted line frame. When the aging temperature is 500 °C, the dimple size in the microscopic fracture is uniform and dense. Moreover, as the aging temperature increases, the dimple size becomes larger. When the aging temperature increases to 650 °C, the macro fracture is deformed and cracks appear. In addition, the strength is decreased, which is closely related to the thickness of the  $\alpha_s$  phase.

Fig.11 shows the impact and tensile fracture morphologies of Ti6321 alloy after aging at 600 °C for different time. According to Fig.11a and Fig.11d, it can be seen from the macro fracture of the impact sample that the material shows ductile fracture. Fig.11a<sub>1</sub> and Fig.11d<sub>1</sub> show the enlarged images of the position of the white dotted line frame. With the increase in aging temperature, micropores in the impact fracture gradually increase and cracks gradually appear, as shown in Fig.11c<sub>1</sub>. When the aging temperature is 600 °C and the aging time is 12 h, the impact and tensile samples have the least microvoids, and the number of dimples is large and the size is uniform, so they show good impact toughness and strength.

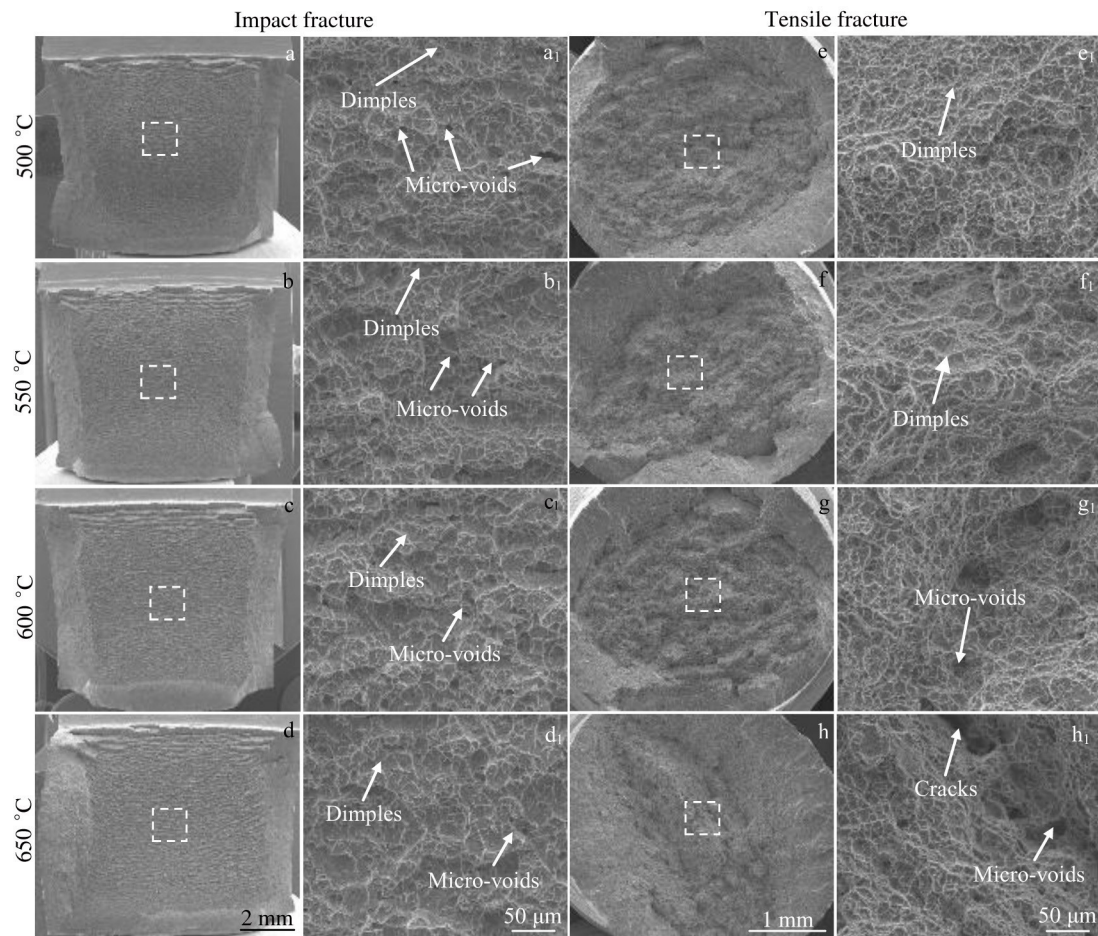


Fig.10 Impact and tensile fracture morphologies of Ti6321 alloy after aging at different temperatures for 6 h

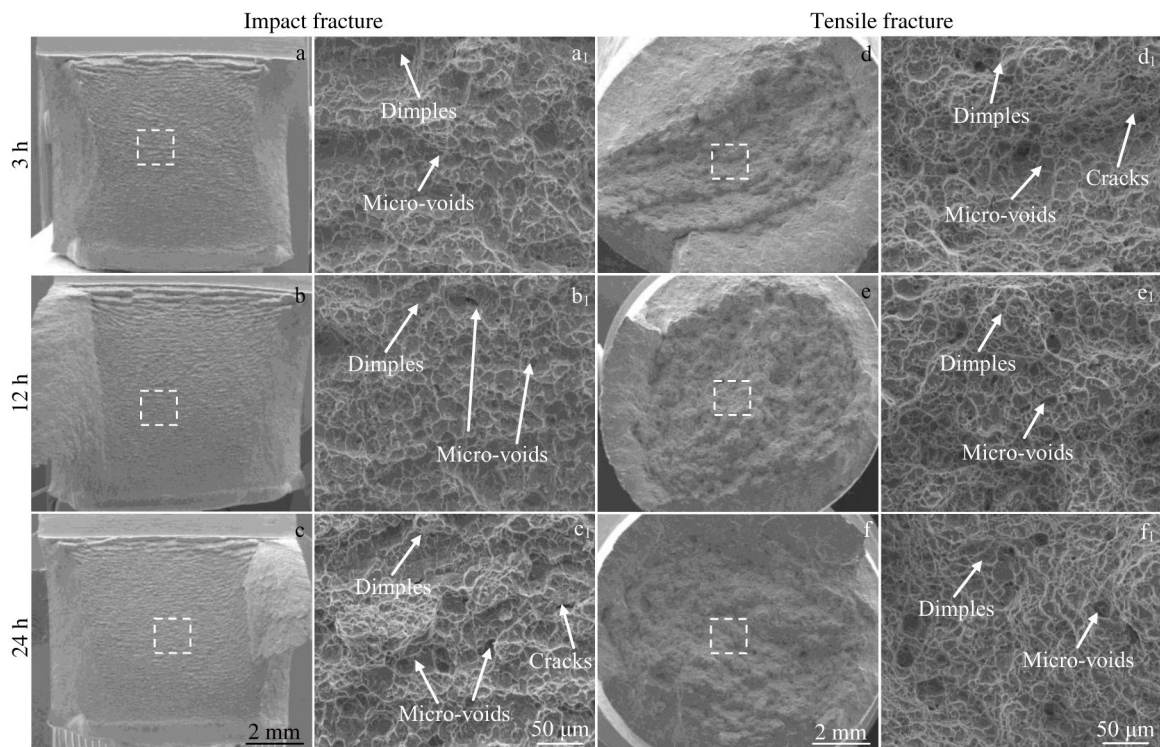


Fig.11 Impact and tensile fracture morphologies of Ti6321 alloy after aging at 600 °C for different time

### 3 Conclusions

1) In the Ti6321 alloy, the  $\alpha_s$  phase is more sensitive to aging parameters. The thickness of  $\alpha_s$  phase is positively correlated with aging temperature or time. As the aging temperature and aging time increase, the segregation of Ti and Al elements in  $\beta_1$  phase is obvious, and the  $\alpha_s$  phase in  $\beta_1$  phase changes from fine needle-like to long rod-like.

2) Mechanical properties are more sensitive to aging temperature than to aging time. As the aging temperature increases, the yield and tensile strength decrease and the impact energy increases. When the alloy is aged at 600 °C for 12 h, the comprehensive performance reaches to the best. The tensile strength, yield strength, and elongation are 907 MPa, 796 MPa, and 16%, respectively. Meanwhile, the impact energy is 55 J.

3) The tensile and impact toughness fracture of Ti6321 alloy are ductile after aging treatment. The coarsened  $\alpha_s$  phases increase the crack propagation resistance during the impact process and make the expansion path tortuous, but the coarsened  $\alpha_s$  phase is not conducive to the tensile properties of the alloy.

### References

- Zhu Shunpeng, Liu Qiang, Peng Weiwen et al. *International Journal of Mechanical Sciences*[J], 2018, 142–143: 502
- Arba A, Chen Pengwan, Guo Yansong. *Mechanics of Materials*[J], 2019, 137: 103–121
- Lin Yongcheng, Tang Yi, Zhang Xiaoyong et al. *Vacuum*[J], 2019, 159: 191
- Popov A A. *Metal Science and Heat Treatment*[J], 1995, 37: 409
- Xiong Jinhui, Li Shikai, Gao Fuyang et al. *Materials Science and Engineering A*[J], 2015, 640: 419
- Guo Kai, Meng Kang, Miao Dun et al. *Materials Science and Engineering A*[J], 2019, 766: 138–146
- Wang Qi, Ren Junqiang, Wu Yukun et al. *Journal of Alloys and Compounds*[J], 2019, 789: 249
- Yin Lixia, Liang Shunxing, Zheng Liyun. *World Journal of Engineering*[J], 2015, 12(4): 319
- Li Juan, Xu Yaqun, Xiao Wenlong et al. *Journal of Materials Science & Technology*[J], 2022, 109: 1
- Bobbili R, Ramudu B V, Madhu V. *Journal of Alloys and Compounds*[J], 2017, 696: 295
- Wen Xin, Wan Mingpan, Huang Chaowen et al. *Materials & Design*[J], 2019, 180: 107–116
- Ei-hadad S, Nady M, Khalifa W et al. *Canadian Metallurgical Quarterly*[J], 2017, 57(2): 186
- Du Zhaoxin, Xiao Shulong, Xu Lijuan et al. *Materials & Design*[J], 2014, 55: 183
- Wang Ke, Zhao Yongqing, Jia Weiju et al. *Rare Metal Materials and Engineering*[J], 2021, 50(2): 552
- Sadeghpour S, Abbasi S M, Morakabati M et al. *Materials & Design*[J], 2017, 121: 24
- Xavier C C, Correa D R N, Grandini C R et al. *Journal of Alloys and Compounds*[J], 2017, 727: 246
- Wu Songquan, Lu Yanjin, Gan Yiliang et al. *Journal of Alloys and Compounds*[J], 2016, 672: 643
- Zhu Yanyan, Chen Bo, Tang Haibo et al. *Transactions of Nonferrous Metals Society of China*[J], 2018, 28: 36
- Zhou L, Chang M L, Dong L et al. *Materials Research Innovations*[J], 2014, 19(S4): 929
- Shekhar S, Sarkar R, Kar S K et al. *Materials & Design*[J], 2015, 66: 596
- Wang Fang, Lei Liming, Fu Xin et al. *Materials Science and Engineering A*[J], 2020, 782: 139–148
- Yue Ke, Liu Jianrong, Zhu Shaoxiang et al. *Materialia*[J], 2018, 1: 128
- Shi Xiaohui, Zeng Wendong, Long Yu et al. *Journal of Alloys and Compounds*[J], 2017, 727: 555
- Chen Yuyong, Du Zhaoxin, Xiao Shulong et al. *Journal of Alloys and Compounds*[J], 2014, 586: 588
- Fan Jiangkun, Li Jinshan, Kou Hongchao et al. *Materials & Design*[J], 2015, 83: 499
- Wu Chuan, Zhan Mei. *Transactions of Nonferrous Metals Society of China*[J], 2019, 29(5): 997
- Xu Wujiao, Tan Yuquan, Gong Lihua et al. *Rare Metal Materials and Engineering*[J], 2016, 45(11): 2932
- Wu Chuan, Zhan Mei. *Journal of Alloys and Compounds*[J], 2019, 805: 1144

## 时效处理对 Ti-6Al-3Nb-2Zr-Mo 合金组织演变和力学性能的影响

江海洋<sup>1,2,3</sup>, 江福清<sup>2,3</sup>, 王冰<sup>1,2,3</sup>, 徐斌<sup>1,3</sup>, 孙明月<sup>1,3</sup>

(1. 中国科学院金属研究所 核材料与安全评估重点实验室, 辽宁 沈阳 110016)

(2. 中国科学技术大学 材料科学与工程学院, 辽宁 沈阳 110016)

(3. 中国科学院金属研究所 沈阳材料科学国家实验室, 辽宁 沈阳 110016)

**摘要:** 为了解不同时效参数对 Ti-6Al-3Nb-2Zr-Mo (Ti6321) 合金组织和力学性能影响的根本原因, 通过光学显微镜 (OM)、扫描电镜 (SEM)、透射电镜 (TEM) 和力学性能测试, 研究了不同时效条件 (500~650 °C, 3~24 h) 下的显微组织和力学性能。结果表明, 次生相  $\alpha_s$  比初生相  $\alpha_p$  对时效参数更为敏感。此外,  $\alpha_s$  相的厚度与时效温度和时效时间呈正相关。随着时效温度和时效时间的增加, Ti 和 Al 元素在  $\beta_1$  相中的偏析明显,  $\alpha_s$  相由细针状转变为长棒状。当合金在 600 °C 时效 12 h 时, 合金表现出较好的综合力学性能。抗拉伸强度、屈服强度和伸长率分别为 907 MPa、796 MPa 和 16%, 冲击功为 55 J。

**关键词:** Ti-6Al-3Nb-2Zr-Mo 钛合金; 时效处理; 微观结构演化; 力学性能

作者简介: 江海洋, 男, 1992 年生, 博士, 中国科学院金属研究所, 辽宁 沈阳 110016, 电话: 024-83971973, E-mail: hyjiang19b@imr.ac.cn